# We are IntechOpen,
## the world's leading publisher of Open Access books
## Built by scientists, for scientists

## 6,900
Open access books available

## 186,000
International authors and editors

## 200M
Downloads

Our authors are among the

## 154
Countries delivered to

## TOP 1%
most cited scientists

## 12.2%
Contributors from top 500 universities

CLARIVATE ANALYTICS
**BOOK CITATION INDEX**
INDEXED

**WEB OF SCIENCE**™

Selection of our books indexed in the Book Citation Index
in Web of Science™ Core Collection (BKCI)

## Interested in publishing with us?
## Contact book.department@intechopen.com

Numbers displayed above are based on latest data collected.
For more information visit www.intechopen.com

# Study of SiO$_2$/Si Interface by Surface Techniques

Constantin Logofatu, Catalin Constantin Negrila,
Rodica V. Ghita, Florica Ungureanu, Constantin Cotirlan,
Cornelui Ghica Adrian Stefan Manea and Mihai Florin Lazarescu
*National Institute of Materials Physics, Bucharest*
*Romania*

## 1. Introduction

Due to its dominant role in silicon devices technologies [1, 2] the SiO$_2$/Si interface has been intensively studied in the last five decades. The ability to form a chemically stable protective layer of silicon dioxide (SiO$_2$) at the surface of silicon is one of the main reasons that make silicon the most widely used semiconductor material. This silicon oxide layer is a high quality electrically insulating layer on the silicon surface, serving as a dielectric in numerous devices that can also be a preferential masking layer in many steps during device fabrication. Native oxidation of silicon is known to have detrimental effects on ultra-large-scale integrated circuit (ULSIC) processes and properties including metal/silicon ohmic contact, the low-temperature epitaxy of silicide and dielectric breakdown of thin SiO$_2$ [3]. The use of thermal oxidation of Si(100) to grow very thin SiO$_2$ layers (~ 100Å) with extremely high electrical quality of both film and interface is a key element on which has been built the success of modern MOS (metal-oxide-semiconductor) device technology [4]. At the same time the understanding of the underlying chemical and physical mechanisms responsible for such perfect structures represents a profound fundamental challenge, one which has a particular scientific significance in that the materials (Si, O) and chemical reaction processes (e.g. thermal oxidation and annealing) are so simple conceptually.

As a result of extreme decrease in the dimensions of Si metal-oxide-semiconductor field effect transistor device (MOSFET), the electronic states in Si/SiO interfacial transition region playa vital role in device operation [5]. The existence of abrupt interfaces, atomic displacements of interface silicon and intermediate oxidation states of silicon are part of different experiments [6, 7]. The chemical bonding configurations deduced from the observed oxidation states of silicon at the interface are the important basis for the understanding of the electronic states. The distribution of the intermediate oxidation states in the oxide film and the chemical bonding configuration at the interface for Si(100) and Si(111) were investigated [5] using measurements of Si 2p photoelectron spectra. One of the X-ray photoelectron spectroscopy (XPS) results is that the difference for <100> and <111> orientations is observed in the intermediate oxidation state spectra. Ultra thin SiO$_2$ films are critical for novel nanoelectronic devices as well as for conventional deep submicron ULSIC where the gate oxide is reduced to less than 30Å. Precise thickness measurement of these

ultra thin films is very critical in the development of Si- based devices. Oxide thickness is commonly measured by ellipsometry [8] but as film thicknesses is scaled down to several atomic layers, surface analytical techniques such as XPS become applicable tools to quantify these films [9]. An XPS measurement offers the additional advantage of providing information such as surface contamination and chemical composition of the film.

The purpose of the present section is to study the chemical structure modifications at the surface on semiconductors (e.g. Si, GaAs) by XPS, (angle resolved XPS) ARXPS and (scanning tunneling microscopy) STM techniques. It will be studied the variation of the interface for native oxides and for thermally grown oxides. This analysis will be the base for *in situ* procedures in the development of different devices as Schottky diodes or in the technique of local anodic oxidation (LAO) [10] for fabricating electronic devices on a nanometer scale.

A silicon dioxide layer is often thermally formed in the presence of oxygen compounds at a temperature in the range 900 to $1300^0$C. There exist two basic means of supplying the necessary oxygen into the reaction chamber. The first is in gaseous pure oxygen form (dry oxidation) through the reaction: $Si+O_2 \rightarrow SiO_2$. The second is in the form of water vapor (wet oxidation) through the reaction: $Si+2H_2O \rightarrow SiO_2+2H_2$. For both means of oxidation, the high temperature allows the oxygen to diffuse easily through the silicon dioxide and the silicon is consumed as the oxide grows. A typical oxidation growth cycle consists of dry-wet-dry oxidations, where most of the oxide is grown in the wet oxidation phase. Dry oxidation is slower and results in more dense, higher quality oxides. This type of oxidation method is used mostly for MOS gate oxides. Wet oxidation results in much more rapid growth and is used mostly for thicker masking layers. Before thermal oxidation, the silicon is usually preceded by a cleaning sequence designed to remove all contaminants. Sodium contamination is the most harmful and can be reduced by incorporating a small percentage of chlorine into the oxidizing gas. The cleaned wafers are dried and loaded into a quartz wafer holder and introduced in a furnace. The furnace is suitable for either dry or wet oxidation film growth by turning a control valve. In the dry oxidation method, oxygen gas is introduced into the quartz tube. High-purity gas is used to ensure that no impurities are incorporated in the oxide layer as it forms. The oxygen gas can also be mixed with pure nitrogen in order to decrease the total cost of oxidation process. In the wet oxidation method, the water vapor introduced into the furnace system is usually creating by passage a carrier gas into a container with ultra pure water and maintained at a constant temperature below its boiling point ($100^0$C). The carrier gas can be either nitrogen or oxygen and both result in equivalent oxide thickness growth rates.

The structure of $SiO_2$/Si interface has been elusive despite many efforts to come up with models. Previous studies [11-13] generally agree in identifying two distinct regions. The near interface consists of a few atomic layers containing Si atoms in intermediate oxidation states i.e. $Si^{1+}$ ($Si_2O$), $Si^{2+}$ ($SiO$) and $Si^{3+}$ ($Si_2O_3$). A second region extends about 30Å into $SiO_2$ overlayer. The $SiO_2$ in this layer is compressed because the density of Si atoms is higher for Si than for $SiO_2$. Different structural models [14-17] have been proposed for $SiO_2$ on Si (100), each predicting a characteristic distribution of oxidation states, and most of the models assume an atomically abrupt interface. From experiments was observed [1] at interface the existence of a large portion of $Si^{3+}$, and the model in accord this observation is that of an extended-interface for $SiO_2$/Si (100) by minimizing the strain energy [17]. Relatively new models ('90 years) are based for $SiO_2$/Si (100) and $SiO_2$/Si (111) on the distribution and intensity of intermediate oxidation states. These models are characterized by an extended interface with protrusions of $Si^{3+}$ reaching about 3 Å into the $SiO_2$ overlayer.

Experimental techniques as the one presented in this work were used to determine the structure of the interface, its extend and to appreciate its roughness.

## 2. Investigation techniques

*X-ray Photoelectron Spectroscopy (XPS)* technique offers several key features which makes it ideal for structural and morphological characterization of ultra-thin oxide films. The relatively low kinetic energy of photoelectrons (< 1.5 keV) makes XPS inherently surface sensitive in the range (1-10 nm). Secondly, the energy of the photoelectron is not only characteristic of the atom from which it was ejected, but also in many cases is characteristic of the oxidation state of the atom (as an example the electrons emitted from $2p_{3/2}$ shell in $SiO_2$ are present approximately 4 eV higher in binding energy than electrons from the same shell originating from $Si^0$ (bulk Si). In the third place the XPS has the advantage that is straightforward to quantify through the use of relative sensitivity factors that are largely independent of the matrix.

The XPS recorded spectra were obtained using SPECS XPS spectrometer based on Phoibus analyzer with monochromatic X-rays emitted by an anti-cathode of Al (1486.7 eV). The complex system of SPECS spectrometer presented in Fig.1 allows the ARXPS analysis, UPS and STM as surface investigation techniques.
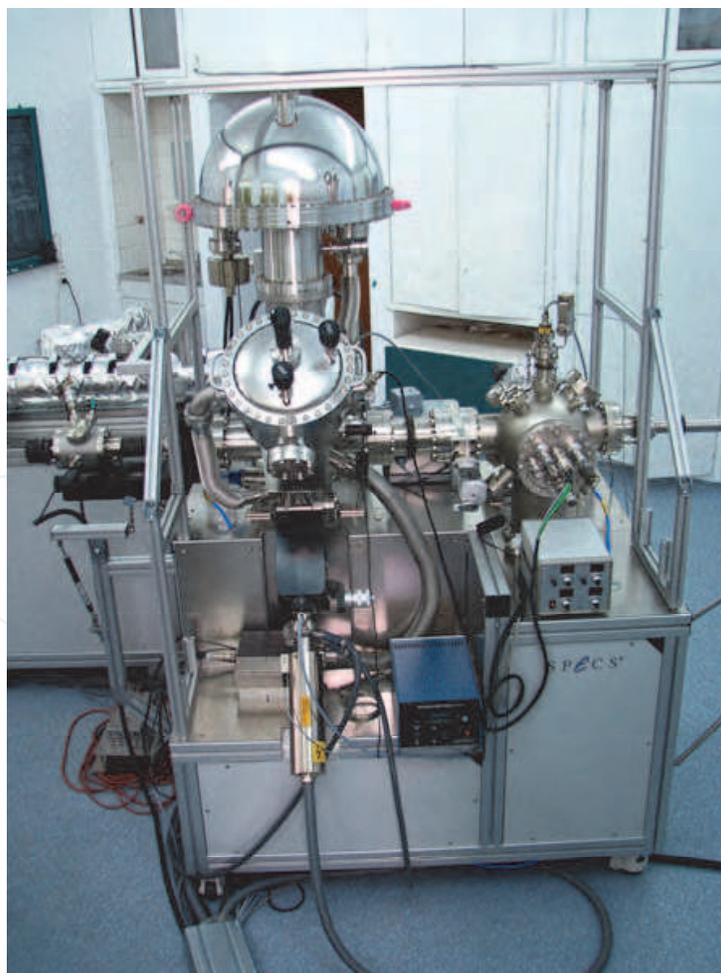


Fig. 1. SPECS complex system for surface analysis

A hemispherical analyzer was operated in constant energy mode with a pass energy of 5 eV giving an energy resolution of 0.4 eV, which was established as FWHM (full width half maximum) of the Ag 3d5/2 peak. The analysis chamber was maintained in ultra high vacuum conditions (~ $10^{-9}$ torr). As a standard practice in some XPS studies  the C (1s) line (285 eV) corresponding to the C-C line bond had been used as reference Binding Energy (BE) [18]. The recorded XPS spectra were processed using Spectral Data Procesor v 2.3 (SDP) software. In its structure the SDP soft uses the deconvolution of a XPS line as a specific ratio between Lorentzian and Gaussian line shape and these characteristics ensures a good fit of experimental data.

*Angle resolved X-ray Photoelectron Spectroscopy (ARXPS)* is related to a XPS analysis of recorded spectra on the same surface at different detection angles θ of photoelectrons measured to the normal at the surface. The analysis chamber is maintained at ultra-high vacuum (~ $10^{-9}$ torr) and the take-off-angle (TOA) was defined in accord to ASTM document E 673-03 related to standard terminology related to surface analysis that describes TOA as the angle at which particles leave a specimen relative to the plane of specimen surface; it is worth to mention that our experimental measured angle is congruent with TOA as angles with correspondingly perpendicular sides. For a detection angle θ, the depth λ from where it proceeds the XPS signal is given by the projection of photoelectrons pass $\lambda_m$ (the maximum escape depth) on the detection direction:

$$\lambda = \lambda_m \cos\theta$$

In Fig.2 is presented the TOA angle considered in the equation for oxide thickness evaluation as presented in [3, 19, 20, and 21].
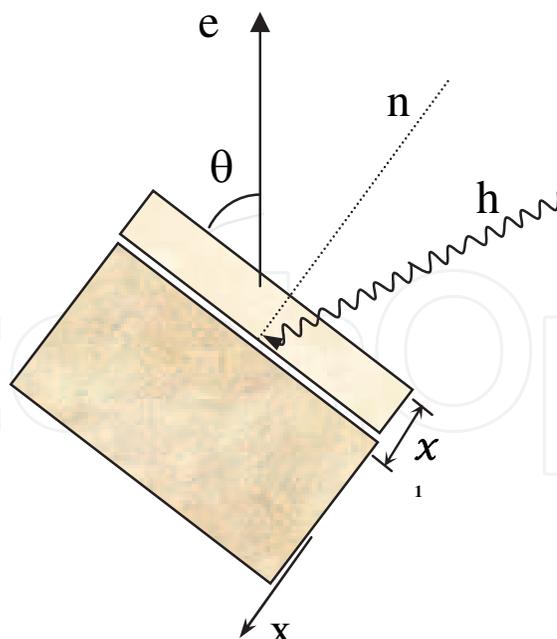


Fig. 2. Sample characteristics in ARXPS measurement

The oxide film thickness $d_{oxy}$ is determined by the Si 2p core level intensity ratio of the oxidized silicon film $I_{oxy}$ and substrate silicon $I_{si}$ by:

$$d_{oxy}=\lambda_{oxy}\sin\theta[I_{oxy}/(\alpha I_{Si})+1] \qquad (1) \quad \text{reference [9]}$$

where

$$\alpha=I_{oxide\infty}/I_{si\infty} = 0.76 \qquad (2)$$

The value for this ratio was experimentally obtained taking into account the intensity for the line $SiO_2$ ($Si^{4+}$) in a thick layer of oxide (where the signal for the bulk silicon is not present) reported to the intensity of $Si^0$ line in bulk silicon (where the oxide do not exists e.g. after $Ar^+$ ion sputtering).

It is well known however that large discrepancies exist for the photoelectron effective attenuation length in $SiO_2$ where values from 2 to 4 nm have been reported and compared to theoretical prediction for the inelastic mean free path. The ARXPS measurements are dependent on the value of $\sin\theta$, and the ratio $I_{oxy}/I_{Si}$ will be computed only for $SiO_2$ oxide ($Si^{4+}$). The electron inelastic mean free path (IMFP) $\lambda$ is analyzed and computed in terms of the Bethe equation for inelastic scattering which can be written [22]:

$$\lambda=E/\ [E_p^2\beta\ \ln(\gamma E)]\ \text{Å} \qquad (3)$$

For electrons in the range (50-200) eV [7, 8] the computed IMFP is presented in the form of TPP-2M formula:

$$\lambda=E/\ \{E_p^2\ [\beta\ln(\gamma E)-C/E+D/E^2]\} \qquad (4)$$

E-electron energy (in eV)
$\beta= -0.10+0.944/\ (E_p^2 + E_g^2) + 0.069\ \rho^{0.1}$

$$\gamma= 0.191\ \rho^{-0.50} \qquad (5)$$

C= 1.97- 0.91 U
D= 53.4 – 20.8 U
U = $N_V\rho/$ A   ($N_V$- total number of valence electrons per atom or molecule,  $\rho$- density (gcm$^{-3}$), A- atomic or molecular weight, $E_g$-band gap, $E_p$- plasmon energy)

For $E_p$ which is the free- electron plasmon energy (in eV) it was used the formula

$$E_p= 28.8\ (\rho N_V/A\ )^{1/2}\ \text{eV} \qquad (6)$$

as is mentioned in reference [21].

For compounds $N_V$ is calculated from the sum of contributions from each constituent element (i.e. $N_V$ for each element multiplied by the chemical or estimated stoichiometric coefficient for that element) [19].

The explored depth of surface layers by XPS technique can be adjusted by the variation of $\theta$ angle.

*Scanning Tunneling Microscopy* (*STM*) is based on the quantum mechanical effect of tunneling. If two metals are brought in close contact and a small voltage is applied between them, a tunneling current can be measured which is:

$$I_t\sim \exp(-2kd) \qquad (7)$$

where d is the distance between the conductors, and as an important message the reason why STM works, is the exponential dependence of the tunneling current on the distance between conductors. Typical values for tunneling voltage are from few mV to several V, and

for the current from 0.5 to 5 nA. The tip-sample distance is a few Angstrom; the tunneling current depends very strongly on this distance. A change of 1 Å causes a change in the tunneling current by a factor of ten. In practice, the tunneling voltage is not always very small. Especially for semiconductors materials a small tunneling voltage can be impossible because there are no carriers in the gap which can be involved in the tunneling. This means that STM can look at both, occupied and unoccupied states of the sample depending on the bias voltage.

*Transmission Electron Microscopy (TEM)*-is a microscopy technique whereby a beam of electrons is transmitted through an ultra thin specimen, interacting with the specimen as it passes through. TEMs are capable of imaging at a significantly higher resolution owing to the small de Broglie wavelength of electrons. This enables the instrument's user to examine fine details-even as small as a single column of atoms. At smaller magnifications TEM image contrast is due to absorption of electrons in the material, due to the thickness and composition of the material.

*UV-Photoelectron Spectroscopy (UPS)*-is the most powerful technique available for probing surface electronic structure. UPS in the laboratory requires a He gas discharge line source which can be operated to maximize the output of either He I (21.2 eV) or He II (40.8 eV) radiation. The use of these photon energies makes accessible only valence levels and very shallow core levels. UPS refers to the measurement of kinetic energy spectra of photoelectrons emitted by ultraviolet photons, to determine molecular energy levels in the valence region [23]. The kinetic energy $E_K$ of an emitted photoelectron is given by (Einstein law applied to a free molecule):

$$E_K = h\nu - I \qquad (8)$$

Where $h$ is Planck's constant, $\nu$ is the frequency of the ionizing light, and $I$ is an ionization energy corresponding to the energy of an occupied molecular orbital. In the study of solid surfaces in particular is sensitive to the surface region (to 10 nm depth) due to the short range of the emitted photoelectrons (compared to X-rays). A useful result from characterization of solids by UPS is the determination of the work function of the material. The work function $\Phi$ can be defined in terms of the minimum energy $e\Phi$ required to remove an electron from the highest occupied level of a solid to a specified final state. The value of $\Phi$ may depend on distance from the surface on account of the varying electrostatic potential associated with different crystal surfaces.

## 3. Native oxides

Silicon samples Si (100) were exposed to a naturally oxidation process for a long time decade (years) in atmosphere. A thin layer of native oxide was grown, that was firstly put into evidence by a color surface change. In Fig.3 the Si 2p spectra present two lines where the lower binding energy is associated with $Si^0$ (bulk) and the higher binding energy is associated with Silicon dioxide. The Si 2p oxide line intensity increases with the increase in oxide thickness while the Si 2p substrate line intensity decreases [24].

In Fig.4 –are presented the Si 2p lines in crystalline Silicon and in Silicon oxides for the spectra taken at TOA:$25^0$, $55^0$ and $75^0$ for native oxides. As a general remark: in superimposed spectra as the TOA increases the signal from $Si^0$) bulk) is more prominent. For the sample Si (oxidized) the deconvolution for Si core levels 2p lines are related to

specific Binding Energies (BE) for $Si^0$(A), $Si^{1+}$ ($Si_2$O-B), $Si^{2+}$(SiO-C), $Si^{3+}$($Si_2O_3$-D) and $Si^{4+}$($SiO_2$-E) as presented in Fig.5 at TOA= $25^0$.
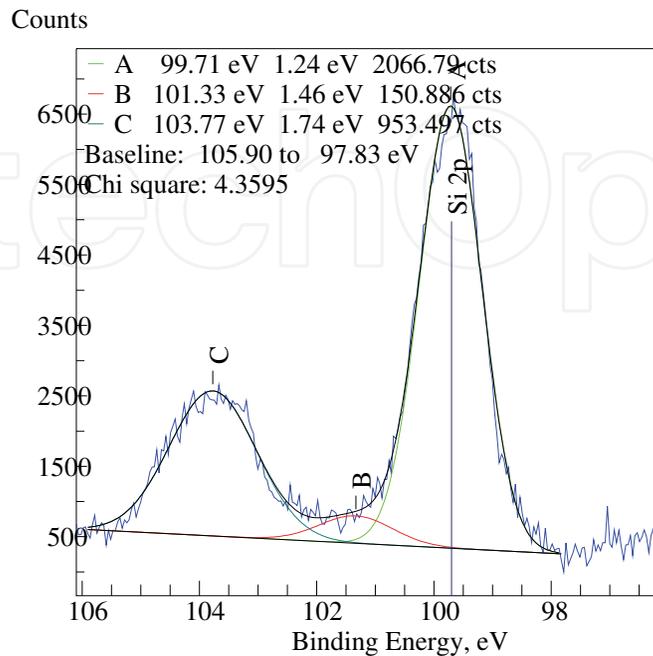


Fig. 3. Si 2p spectra for $Si^{4+}$($SiO_2$-A) and $Si^0$ (bulk-C)
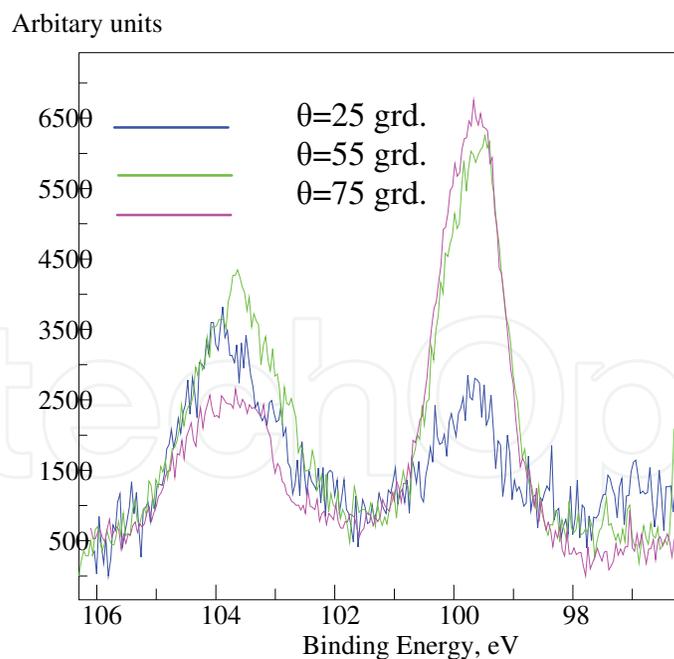


Fig. 4. SiO₂/Si native oxides XPS proportional spectra

As it was mentioned [1] the structure of the interface Silicon Oxide/Silicon consists of two regions. The near interface contains few atomic layers of Si atoms in intermediate oxidation states i.e $Si^{1+}$($Si_2$O), $Si^{2+}$(SiO) and $Si^{3+}$($Si_2O_3$). A second region extends about 30Å into SiO₂ overlayer [1]. As a general remark we assert that although the deconvolution has a slight

arbitrary degree in S0 sample, it prevails the sub oxides with high oxidation states (e.g. $Si^{3+}$). Regarding the measurement of oxide thickness the ratio $I_{oxy}/I_{Si}$ in the oxidation state $Si^{4+}$ ($SiO_2$) can be evaluated for the sample S0 and the computed value is in accord with the presented theory of Electron Inelastic Mean Free Path (IMFP) as presented in literature since 1994, and conduced to the value $d_{oxy} \sim 23.6$Å for native oxide.
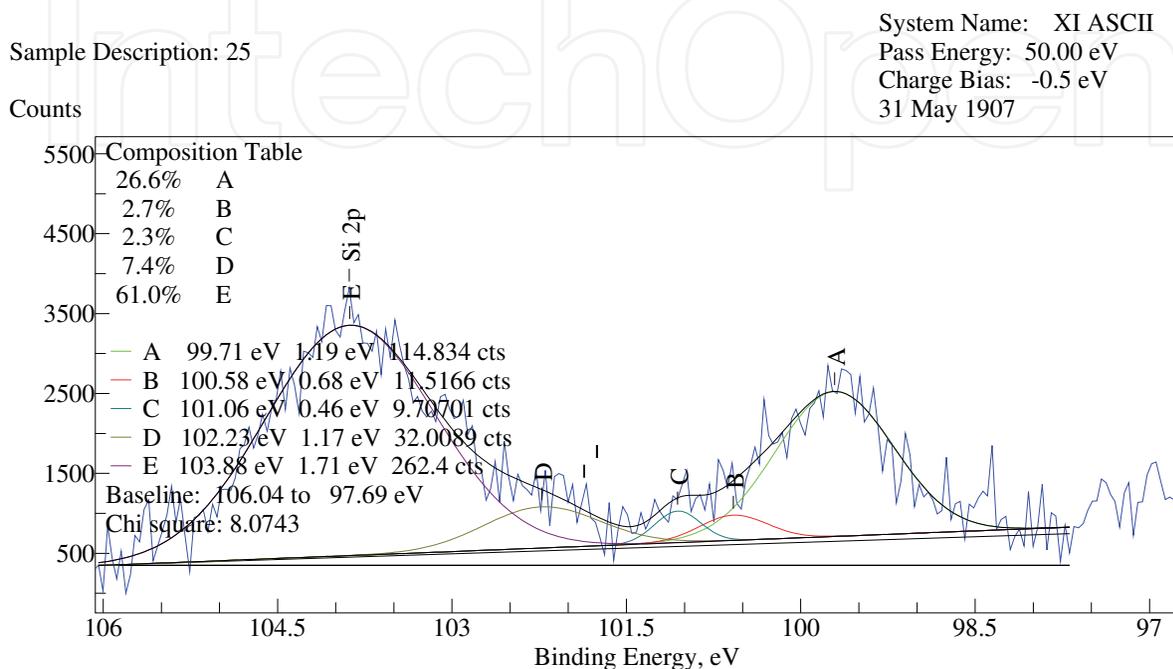


Fig. 5. XPS spectra for Si (oxidized) S0 sample at TOA=25⁰

| Oxidation states for Si | Results in our experiment BE(eV) | BE(eV) Reference[1] | Composition table (%) |
|---|---|---|---|
| $Si^0$ | 99.7 | 99.5 | 26.6 |
| $Si^{1+}$ | 100.58 | 100.45 | 2.7 |
| $Si^{2+}$ | 101.06 | 101.25 | 2.3 |
| $Si^{3+}$ | 102.23 | 101.98 | 7.4 |
| $Si^{4+}$ | 103.88 | 103.40 | 61 |

Table 1. Comparative contribution for Silicon oxides

As an example of a native oxide analysis on semiconductors we present a less extended technological case, the one of GaAs. The GaAs (100) surfaces have a high surface energy [25], and as a consequence they are very reactive and chemically unstable. Due to the reactivity of the native oxides is difficult to reach the passivation of GaAs surfaces. Bare arsenic atoms are thought to be one of the species present within the native oxides responsible for pinning the Fermi level [26]. The arsenic atoms result from chemistry that occurs at the oxide/GaAs interface. Both $As_2O_3$ and $Ga_2O_3$ will form when a clean GaAs surface is exposed to oxygen and light. The formation of $Ga_2O_3$ is thermodynamically favored and results in the reaction: $As_2O_3 + 2GaAs \rightarrow Ga_2O_3 + 4As$ leaving bare arsenic atoms embedded within the oxide near the oxide/GaAs interface. The $As_2O_3$ is also mobile at grain

boundaries, resulting in a nonuniform oxide in which an As$_2$O$_3$-rich layer is found near the oxide/air interface, and the bare arsenic atoms are found embedded within the Ga$_2$O$_3$-rich layer near the oxide/ GaAs interface. In native oxide layer, both Ga$_2$O$_3$ and As$_2$O$_3$ are somewhat soluble in water and their solubility is dependent on pH. The complicated chemistry of the GaAs native oxides has prevented the development of a simple and robust surface passivation scheme for this surface. IN the ARXPS measurement the Ga and As 3d spectra from the as received (naturally oxidized) GaAs surface taken at TOA: 15$^0$,20$^0$,30$^0$,50$^0$,90$^0$ as presented in Fig. 6 in a proportional ratios. For As, the signal from 41 eV corresponds to As in the volume (GaAs matrix) and the signal near the broad peak of 44 eV is related to As oxides: As$_2$O$_3$ together with As$_2$O$_5$. The As signal from TOA: 15$^0$ is the most sensitive to the surface structure, due to a similar peak intensities arising from oxide (interface) and volume (GaAs).As presented in Fig.7 at small analysis angles the As and Ga
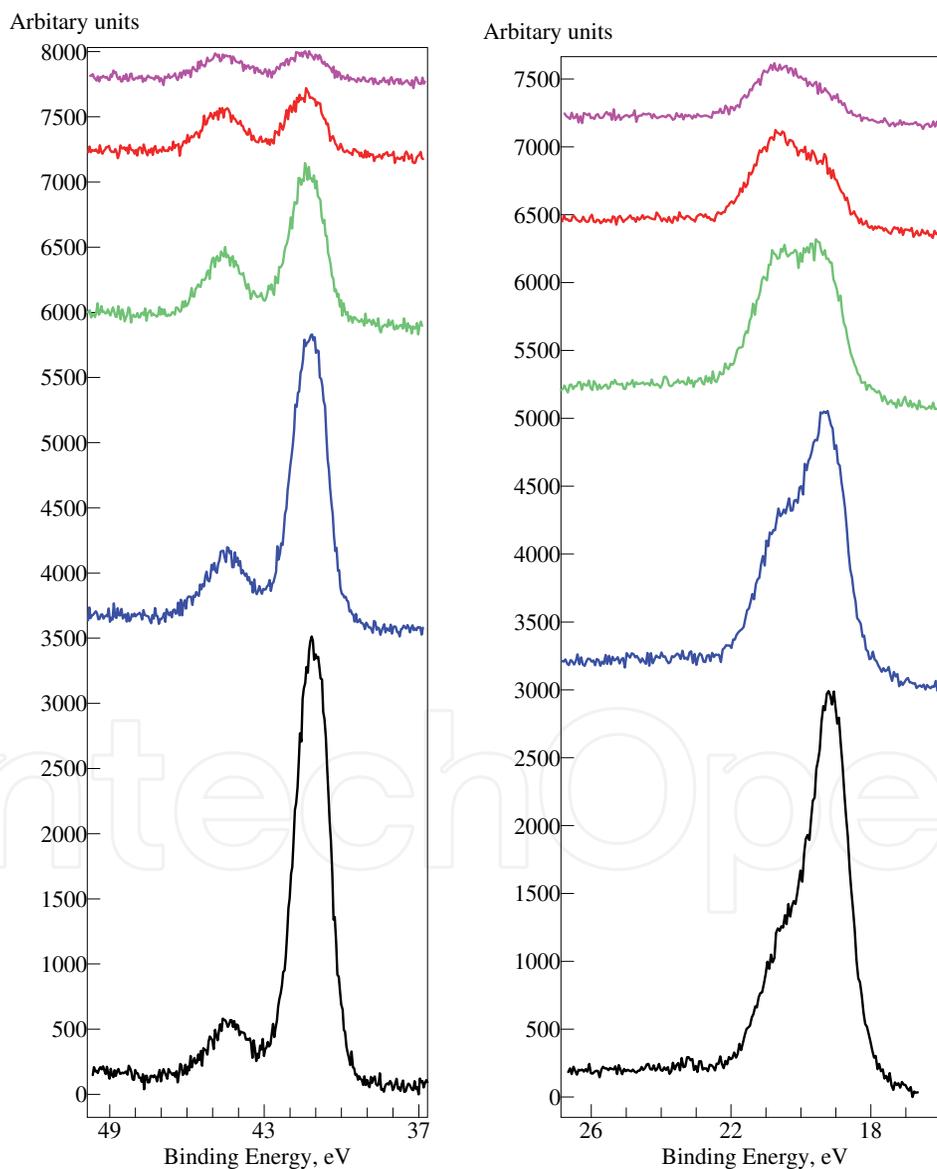


Fig. 6. ARXPS spectra of As 3d (left) and Ga 3d (right) for TOA angles:90$^0$-black, 50$^0$ blue, 30$^0$ –green, 20$^0$-red, 15$^0$-pink

concentrations grows and at the most surface sensitive angle the concentration of C and O is higher than the concentrations for As and Ga. For the native oxidized sample the atomic surface composition Ga/As ratio is related to the entire signal arisen from surface and volume. The Ga signal arises from 19.1 eV (GaAs) and 20.3 eV (Ga$_2$O$_3$) [27]. The As to Ga ratio in the bulk is close to a stoichiometric value of 1.05. For Ga to As ratio in naturally oxidized sample (storage for years) this ratio revealed the contribution of As and Ga from native oxides in the surface layer. The concentration of Ga oxide is greater than of As oxide and from this fact resulted a Ga enrichment in the air exposed GaAs, an observation in accord to reference [28].
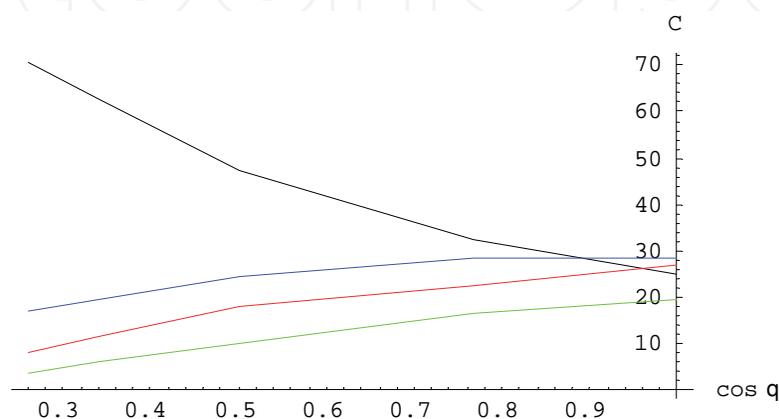


Fig. 7. Relative variation of concentration for C-black, O-blue, As-green and Ga-red as a function of analysis angle (q) (TOA=90$^0$-q)
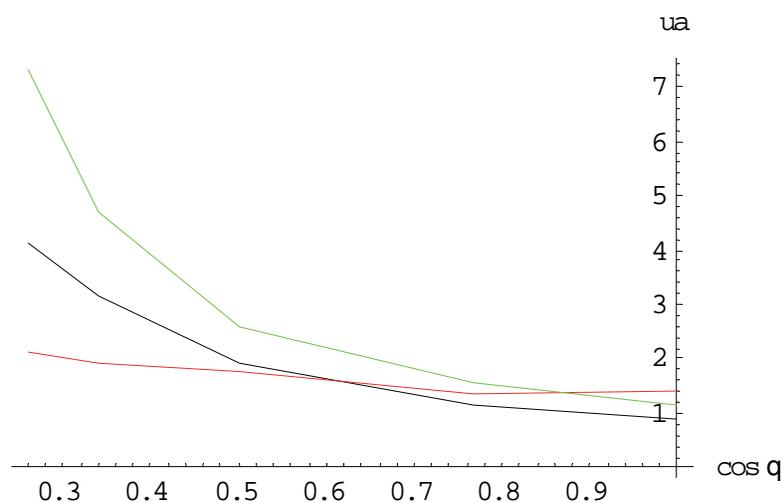


Fig. 8. Variation of different concentration ratios for $C_C/C_O$-black, $C_{Ga}/C_{As}$-red, $C_c+C_O/C_{Ga}+C_{As}$-green as a function of analysis angle (q) (TOA=90-q)

As can be observed at high TOA angles the concentration ratio $C_C/C_O$ is low and it grows to low TOA angles corresponding to the surface layer. For concentration ratio $C_{Ga}/C_{As}$ on an extended range of angles is constant in a prime approximation, with a slight increase at small TOA angles. The evolution of ratio for contaminants to GaAs ($C_C+C_O/C_{Ga}+C_{As}$) is related to an increase at low TOA angles, as a main result of oxidation to the GaAs surface. We conclude that the surface native oxide comprise a mixture of Ga$_2$O$_3$, As$_2$O$_3$ and As$_2$O$_5$ phases

## 4. Silicon/oxide interface

The Silicon oxide samples were prepared for different analysis by cleaning in organic solvents, and chemical etching in aqueous solution of hydrofluoric acid. There were examined samples exposed to air oxidation for a long period of time together with samples maintained for 2-3 hours in atmosphere after a chemical etching as well as chemical etched fresh samples. In this experiment there were used as substrates p-Si (100) and p-Si (111) of medium resistivity. The ARXPS spectrum of O 1s and C 1s are presented in Fig.9
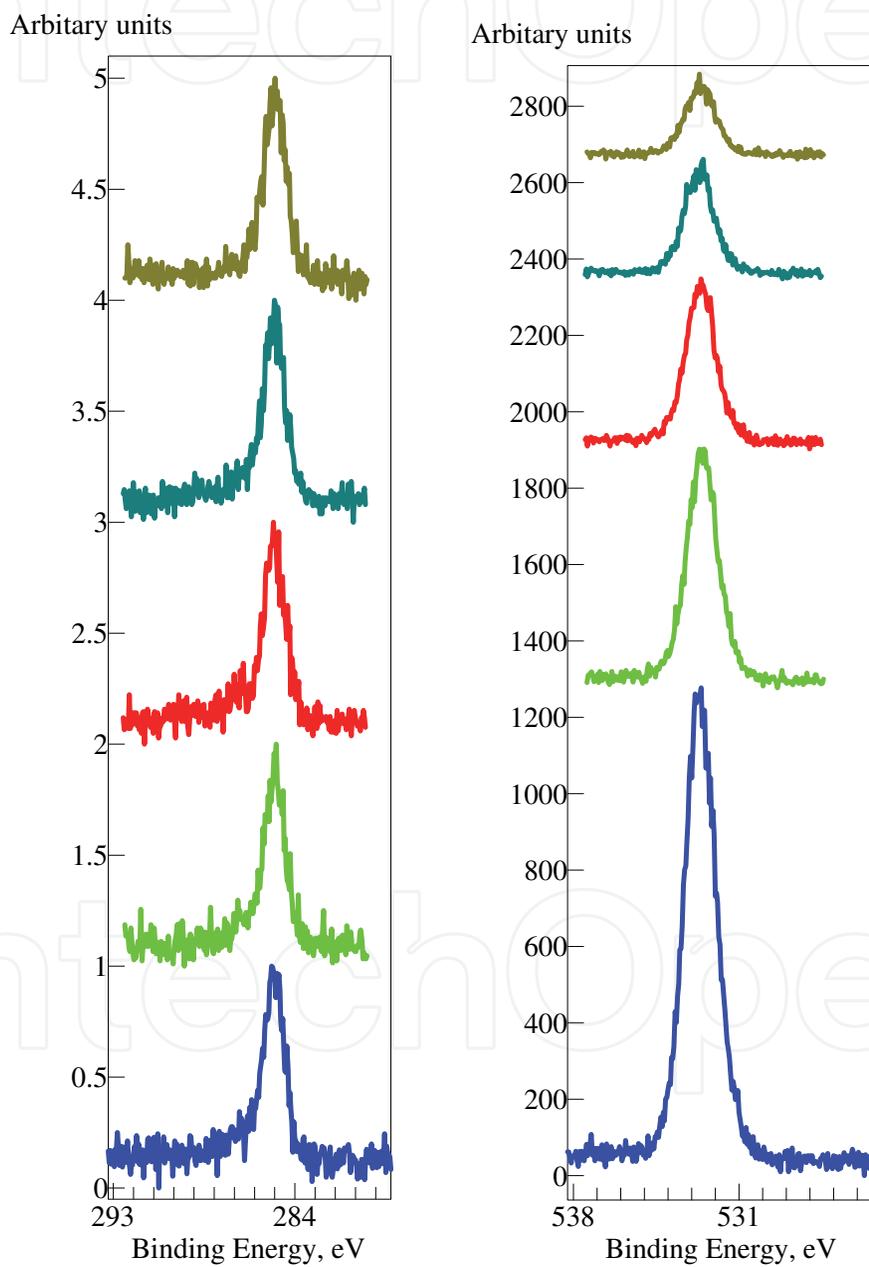


Fig. 9. ARXPS spectra for C1s(left) and O1s (right) at TOA: $90^0$(blue), $50^0$(green), $30^0$(red), $20^0$(turquoise), $15^0$(olive)

The ARXPS spectra of Si 2s and Si 2p for the same sample exposed to natural oxidation is presented in Fig.10
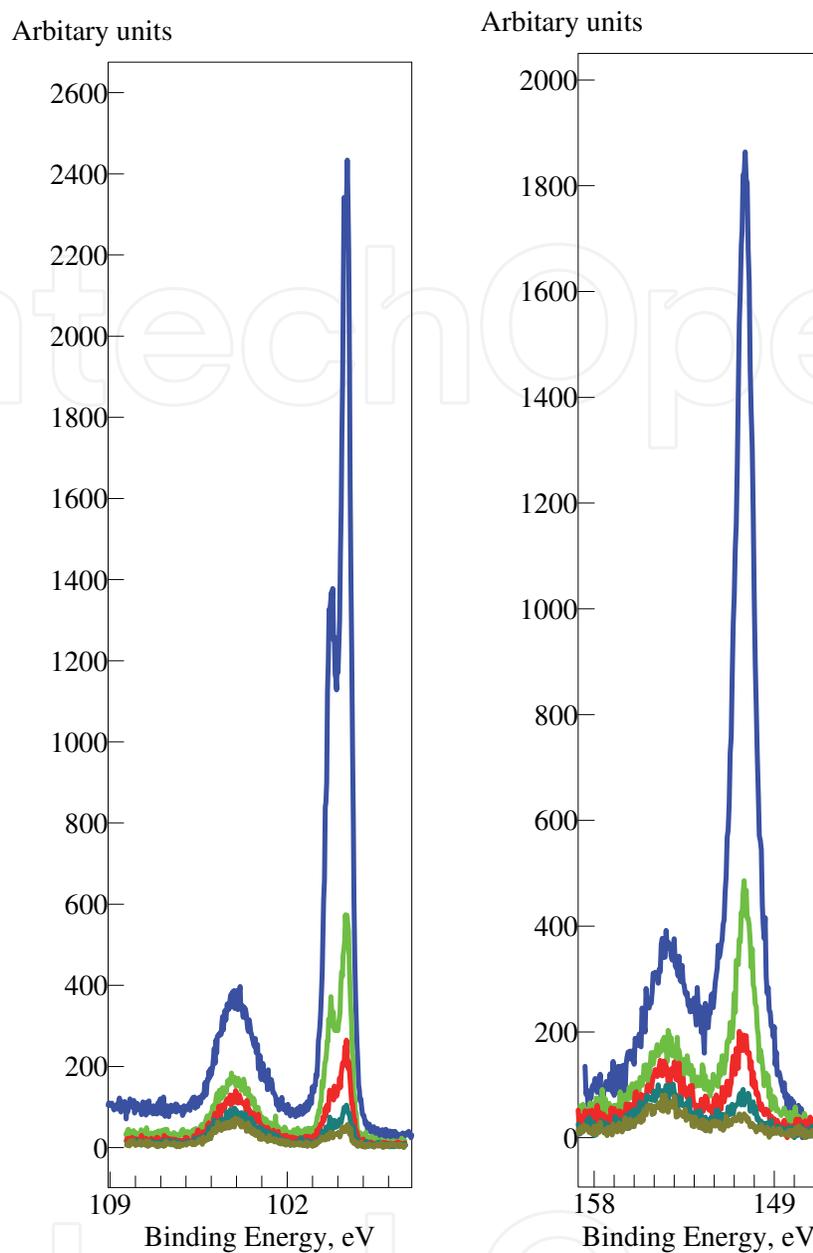
Fig. 10. ARXPS spectra of Si 2s(right) and Si 2p (left) at TOA: $90^0$(blue), $50^0$(green), $30^0$(red), $20^0$(turquoise), $15^0$(olive)

The proposed deconvolution of Si 2p XPS spectra for TOA: $90^0$ and TOA: $15^0$ (the most sensitive angle for the surface composition are presented in Fig.11 (a and b).

The deconvolution for the XPS spectra of Si 2s are presented in Fig.12 (a and b) firstly at TOA:$90^0$, secondly at TOA:$15^0$ as surface sensitive angle.

In Fig.11 (a) the A and B peaks are related to the signal of $Si^0$ 2p ½ and $Si^0$ 2p 3/2, and the peaks of C, D, E and F are related to the signals of sub-oxides as it follows: $Si^{1+}$, $Si^{2+}$, $Si^{3+}$ and $Si^{4+}$. In Fig.11(b) is presented the surface composition for the XPS signal for $Si^0$ 2p1/2 and 2p 3/2 (A and B peaks) and for $Si^{1+}$(C), $Si^{2+}$(D), $Si^{3+}$(E) and $Si^{4+}$(F). The most interesting part of the presented deconvolution is related to the signal of Si 2s that has important similarities with Si 2p spectra, that means in Fig. 12(a) and Fig.12 (b) the presence of $Si^0$ for A peak, and related sub-oxides as follows: $Si^{1+}$ (B), $Si^{2+}$(C), $Si^{3+}$(D), $Si^{4+}$(E). As can be observed in Fig.12

(b) the surface composition is similar as order of magnitude for the signal of Si 2p and Si 2s, and we also notice that the information of XPS spectra related to Silicon/Oxide interface for Si 2s is rare in literature experimental data. For the Binding Energy BE Si 2p3/2= 99.67 eV the shift BE Si 2p3/2 (Si)-BE Si2p3/2 (SiO$_x$) we have the following results: Si$^{1+}$-0.9 eV, Si$^{2+}$-2.1eV, Si$^{3+}$- 3.5eV and Si$^{4+}$-4.5 eV For the Binding Energy BE Si 2s (Si)=150.51 eV the shift BE Si 2s-BE Si 2s (SiO$_x$) we have the following results: Si$^{1+}$-0.97 eV, Si$^{2+}$- 1.79 eV, Si$^{3+}$-2.96 eV, and Si$^{4+}$-4.11 eV.

?
C:\A MRS\2011\04\SI\Si_100_ARXPS\0_Si2p.vms

System Name:   VAMAS
Pass Energy:  5.00 eV
Charge Bias:   0.0 eV
Mon Apr 11 13:00:06 2011

Counts

Composition Table
42.9%   A
21.8%   B
12.2%   C
0.9%   D
1.9%   E
20.3%   F

A   99.66 eV  0.43 eV  173.147 cts
B   100.18 eV  0.51 eV  88.1238 cts
C   100.47 eV  0.74 eV  49.175 cts
D   101.96 eV  1.03 eV  3.73247 cts

Binding Energy, eV
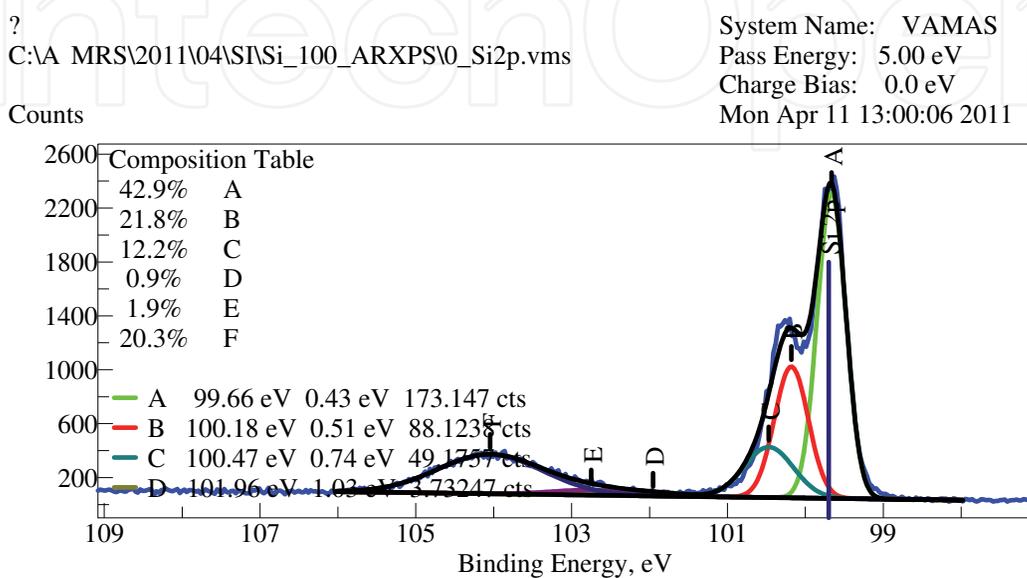
Fig. 11. (a) XPS spectrum of Si 2p at TOA: 90⁰

?
C:\A MRS\2011\04\SI\Si_100_ARXPS\75_Si2p.vms

System Name:   VAMAS
Pass Energy:  5.00 eV
Charge Bias:  -1.4 eV
Mon Apr 11 11:57:23 2011

Counts

Composition Table
13.8%   A
7.3%   B
6.1%   C
2.5%   D
4.6%   E
65.7%   F

A   99.66 eV  0.44 eV  1.28342 cts
B   100.18 eV  0.51 eV  1.72831 cts
C   100.47 eV  0.74 eV  1.45625 cts
D   101.96 eV  1.03 eV  0.590245 cts
E   102.75 eV  1.16 eV  1.08167 cts
F   104.09 eV  1.59 eV  15.5594 cts
Baseline: 107.57 to 98.42 eV
Chi square: 1.1652

Binding Energy, eV

Fig. 11. (b) XPS spectrum of Si 2p at TOA: 15⁰

?
C:\A MRS\2011\04\SI\Si_100_ARXPS\0_Si2s.vms

System Name:   VAMAS
Pass Energy:   5.00 eV
Charge Bias:   -0.5 eV
Mon Apr 11 13:00:37 2011

Counts

Composition Table
67.1%   A
9.7%    B
3.5%    C
6.9%    D
12.8%   E

A   150.45 eV  1.12 eV  254.214 cts
B   151.50 eV  1.14 eV  36.5358 cts
C   152.82 eV  0.94 eV  13.3836 cts
D   153.95 eV  1.35 eV  26.0713 cts
E   154.86 eV  2.18 eV  48.4013 cts
Baseline: 157.98 to 148.03 eV
Chi square: 2.81481

Binding Energy, eV
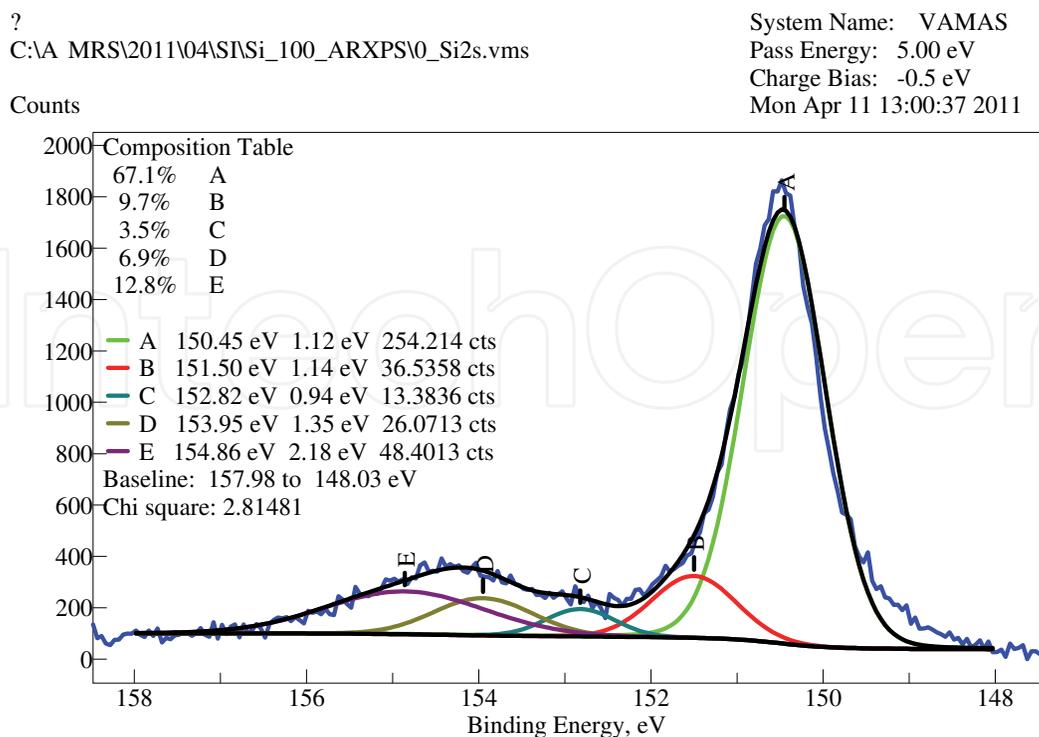
Fig. 12. (a) XPS spectrum 2s at TOA:90$^0$

?
C:\A MRS\2011\04\SI\Si_100_ARXPS\75_Si2s.vms

System Name:   VAMAS
Pass Energy:   5.00 eV
Charge Bias:   0.0 eV
Mon Apr 11 13:00:28 2011

Counts

Composition Table
16.4%    Si 2s (A)
10.5%    Si 2s (B)
6.0%     Si 2s (C)
16.9%    Si 2s (D)
50.2%    Si 2s (E)

A   150.44 eV  1.12 eV  3.74231 cts
B   151.48 eV  1.14 eV  2.40974 cts
C   152.81 eV  0.95 eV  1.36627 cts
D   153.95 eV  1.34 eV  3.85456 cts
E   154.86 eV  2.18 eV  11.4498 cts
Baseline: 158.00 to 148.05 eV
Chi square: 1.5635

Si 2s

Binding Energy, eV

Fig. 12. (b) XPS spectrum 2s at TOA: 15$^0$

In Fig.13 (a) we present the variation of composition with TOA angle that means from bulk (right) to surface (left) for Si, SiO$_x$, and SiO$_2$ for the signal of Si 2p. As can be observed at TOA:90$^0$ the signal of Si$^0$ from the bulk is high and is decreasing near the surface at a

TOA: 15$^0$. At this angle of surface sensitivity the ARXPS signal is related to the presence of oxides, firstly for SiO$_2$ (green) and secondly for SiO$_x$ (blue). In Fig.13 (b) is presented the concentration variation from the bulk to the surface of ARXPS signal for Si 2s. As can be observed the concentration curves for Si$^0$, SiO$_2$ and SiO$_x$ are similar for Si 2p and Si 2s signal. For the ARXPS deconvolutions for Si 2p and Si 2s the positions for Si$^{1+}$- Si$^{4+}$ are matching in the limit of experimental errors.
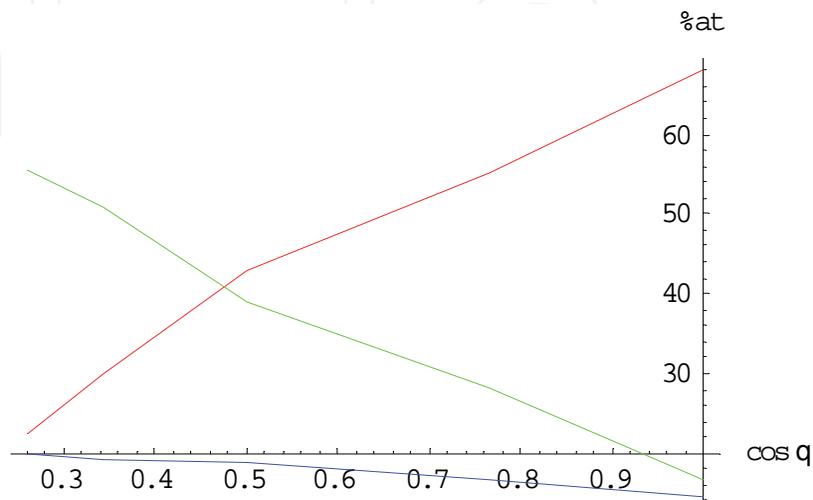


Fig. 13. (a) Concentration variation of Si$^0$(red), SiO$_2$ (green) and SiO$_x$ (blue) at TOA(90$^0$-q) for the ARXPS signal of Si 2p
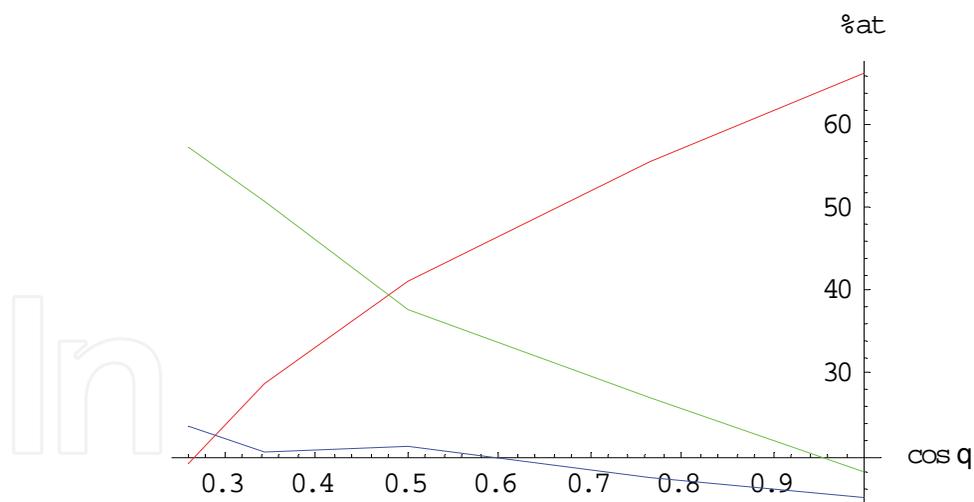


Fig. 13. (b) Concentration variation of Si$^0$(red), SiO$_2$ (green) and SiO$_x$(blue) at TOA (90$^0$-q) for the ARXPS signal of Si 2s

In Fig.14 is presented the variations for different concentration ratios in the surface area for the XPS signal Si (2p) and Si (2s). The proposed experimental concentration ratios are $C_{Si^0}/C_{ox}$, and $C_{Si^{4+}}/C_{SiO_x}$ at different angle orientations in ARXPS signal. As can be observed there is an experimental accord between the ARXPS data between the Si (2p) and Si (2s) data starting from the bulk to the surface, the concentration of Si$^{4+}$ is higher in the surface region, a surface with natural oxidation.

In Fig.15 is present an experimental case of comparison between the XPS spectra of native oxide $SiO_2$ in Si and native $SiO_2$ (quartz) and quartz exposed to different ion etching. In the case of second ion etching it can be observed a shoulder in the XPS signal both on Si (2p) line and Si (2s) line, this shoulder is related to the appearance of a sub-oxide, probably $Si^{3+}$.
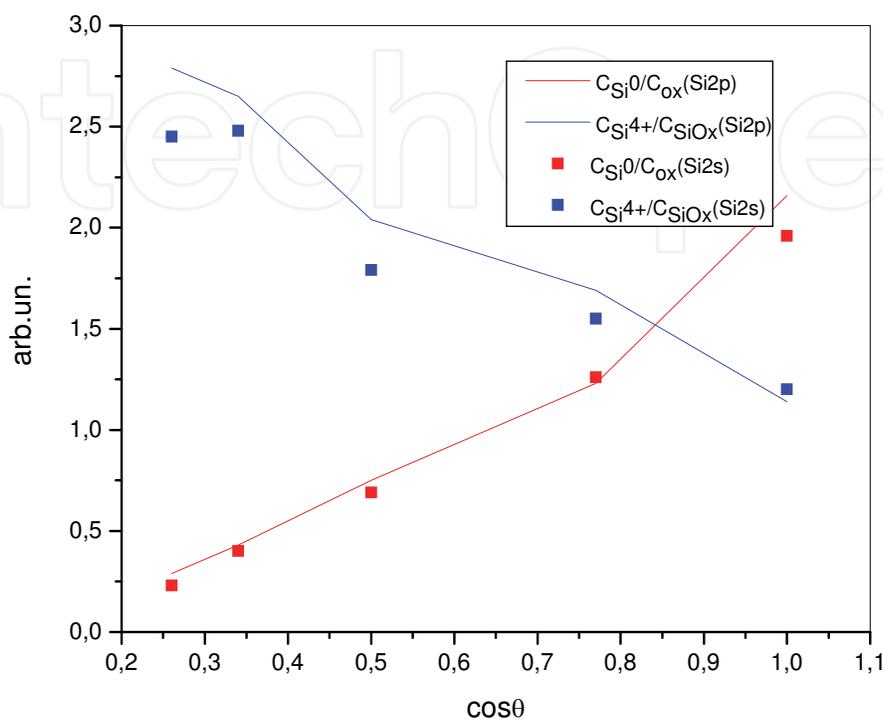


Fig. 14. Variation of concentration ratios for Si (2p) and Si (2s) as a function of TOA ($90^0$-θ)

In principle, the thickness of the native amorphous oxide layer on top of silicon wafers (usually in the range of 2-3 nm) may be directly measured on cross-section images of transmission electron microscopy (TEM). Although the task seems easily achievable, we would like to explain the technical difficulty of the procedure. Cross-section specimens for TEM observations are prepared by gluing against each other fine stripes of Si diced from the original wafer. The obtained sandwich is afterwards mechanically grinded followed by ion milling until a hole is produced in the interface region. The thin border of the created hole represents the useful area for TEM investigations. It is expected that TEM images at high magnification of the wafer surface to reveal the native amorphous layer. The impediment consists in the fact that the assembling resin holding together the two stripes of Si is also amorphous, showing the same contrast as the native amorphous silicon oxide layer, which makes it rather difficult to distinguish the limit between the two amorphous materials in contact.

In our case, a cross section specimen has been prepared from a Si(100) wafer by mechanical grinding and lapping on the two sides of the assembled Si-Si sandwich followed by ion milling at low incidence angle (7 degrees) and 4 kV ion accelerating voltage in a Gatan PIPS installation. The ion milling procedure has been ended with a fine milling step at low voltage (2 kV) in order to remove the amorphous layer created by ion milling and enveloping the surfaces exposed to ion beam. The TEM observation of the prepared specimen has been performed on a JEOL 200CX electron microscope.
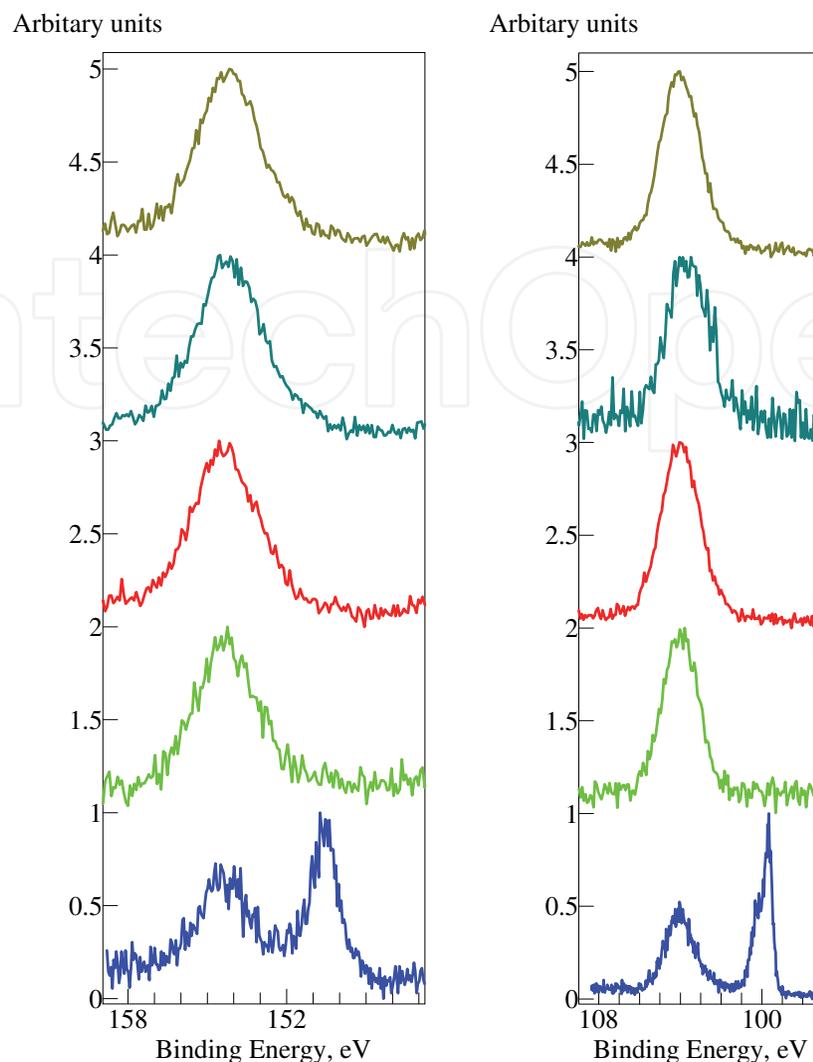
Fig. 15. XPS signal for Si-2p (right) and Si-2s (left) for SiO$_2$/Si (blue), SiO$_2$ (quartz- green), SiO$_2$ ion etching 1(red), SiO$_2$ ion etching 2 (turquoise), SiO$_2$ ion etching 3 (olive)

For a better observation of the amorphous surface layer, the cross-section specimen has been oriented in the microscope along the [110] zone axis as shown in the Selected Area Electron Diffraction pattern inserted in Fig. 16 (a). This way, the strongly diffracting crystalline object, the Si wafer, shows a strong dark contrast, allowing to clearly seeing the interface between the crystalline Si and the amorphous layer on the surface. In the thicker areas of the TEM specimen, the assembling resin has not been removed during the ion milling preparation stage (Fig. 16(a)). Here, the limit between the amorphous SiO$_2$ layer and the amorphous assembling resin is rather difficult to notice. However, the contrast difference between the two amorphous materials allows one to measure the thickness of the SiO$_2$ layer. One can notice the roughness of the crystalline Si wafer and the amorphous band with a rather constant thickness (about 2.5±0.5 nm) running along the surface.

In the thinner areas of the specimen (Fig. 16 ( b)), the assembling resin has been removed by ion milling while a band of amorphous material with the same thickness (2.5±0.5 nm) running parallel to the crystalline surface is still observable.

We conclude, therefore, that the thickness of the amorphous Si layer on top of the Si(001) wafer measured by TEM is 2.5±0.5 nm.
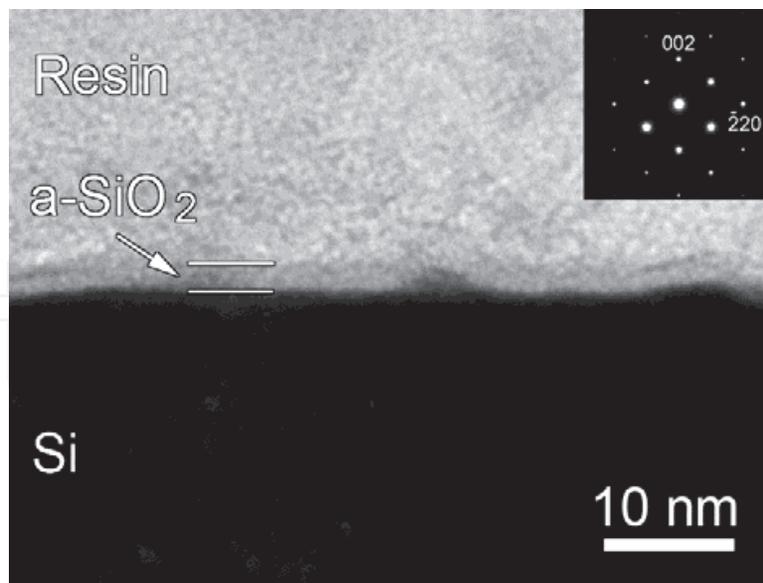
(a)
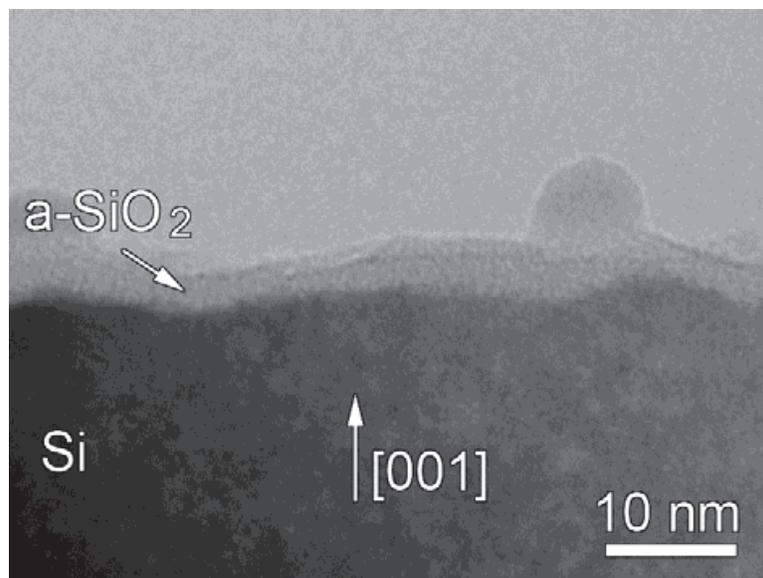


(b)

Fig. 16. (a) Cross-section TEM image of the Si surface in a thicker area of the specimen where the assembling resin is still visible after the ion milling. Inset shows the (b) Cross-section TEM image of the Si surface in a thinner of the specimen, where the assembling resin has been removed by ion milling.

As it was stated in previous works [29, 30, 31] the interface between crystalline Si and its amorphous native oxide $SiO_2$ is the basis for most current computer technology, although its structure is poorly understood. In this line, the study of the structural properties of water near a silica interface by classical and *ab-initio* molecular dynamics simulations is a part of this effort. The orientation of water molecules at the interface determined in classical force fields and quantum simulations [30] show that near the interface the water molecules are oriented such that at least one of the hydrogen atoms are nearer the silica than the oxygen of the water molecule. The importance of characterizing the atomic structure of the

silicon/silicon dioxide interface as an essential component in highly integrated circuits has steadily increased as a result of continuing miniaturization of silicon chips.

## 5. Conclusions

The surface investigations techniques put into evidence the characteristics of Silicon/Oxide interface as it follows:
- the most important result is the XPS analysis of Si (2p) and Si (2s) signals that are similar in the interface region
- the XPS signals of Silicon oxides are related to the oxidation states:Si$^{1+}$, Si$^{2+}$, Si$^{3+}$ and Si$^{4+}$
- the concentration of Si$^{4+}$ is higher in the surface region of natural oxidation
- the result of Ion etching of natural SiO$_2$ (quartz) present the oxidation state Si$^{3+}$
- TEM result put into evidence a region of oxide at the surface that has the properties of the interface including its irregularities, at a thickness of the amorphous Si layer of the Si (001) wafer measured by TEM is 2.5±0.5 nm.

## 6. References

[1] F. J. Himpsel, F.R.Mc Feely, A.Taleb-Ibrahimi and J.A.Yarmoff, *Physical Review B*, Vol.38, No.9, pp.6084-6095 (1988)

[2] M. Razeghi *Technology of Quantum Devices* pp.42 LLC (2010), Springer, ISBN 978-1-4419-1055-4

[3] F. Yano, A.Hiroaka, T.Itoga, H.Kojima and K.Kanehori ,*J.Vac. Sci.Technol A*, Vol.13, No.6 pp.2671 (1995)

[4] G. W. Rubloff, *J.Vac.Sci.Technol. A*, Vol.8, No.3, pp.1857 (1990)

[5] T. Hattori and T.Suzuki, *Appl.Phys.Lett*, Vol.43, No.5 pp.470 (1983)

[6] R. Haight and L.C.Feldman, *J.Appl.Phys*, Vol.53, pp.4884 (1982)

[7] F.J.Grunthaner, P.J. Grunthaner, R.P.Vasquez , B.F.Lewis and J.Maserjian, *J.Vac.Sci.Technol* 16 pp.1443 (1979)

[8] A. Kalnitshi, S.P.Tay, J.P.Ellul, S.Chongsawangvirod, J.W.Andrews and E.A Irene *J.Electrochem. Soc.* 137, pp.235 (1990)

[9] Z. H. Lu, J.P.Mc Caffrey, B.Brar, G.D.Wilk, R.M. Wallace, L.C.Feldman and S.P. Tay, *Appl.Phys Lett.* Vol.71 No.19, pp.2764 (1997)

[10] R. Held, T.Vancura, T.Heinzel, K.Ensslin, M.Holland, W.Wegscheider, *Appl.Phys.Lett*,Vol.73, No.2 pp.262 (1998)

[11] *The physics of SiO$_2$ and its Interfaces* edited by Sokrates T.Pantelides (Pergamon, New York, 1978)

[12] F. J. Grunthaner and P.J.Grunthaner, *Mater, Sci Rep.* 1, pp.65 (1986)

[13] *Proceedings of the 173-rd meeting of the Electrochemical Society*, Atlanta, Georgia, 1988, edited by C.R.Helms

[14] F. Rochet, S.Rigo, M.frament, C.D'Anterroches, C.Maillot, H.Roulet and G.Dufour, *Adv.Phys.* 35, pp.237 (1986)

[15] F. Herman, R.V.Kasowski *J.Vac.Sci.Technol*, 19,pp.395 (1981)

[16] A. Ourmazd, D.W.Taylor, J.A.Rentschles and J.Bevk, *Phys.Rev.Lett*, 59, pp.213 (1987)

[17] L. Ohdomari, H.Akatsu, Y.Yamakoshi and K.Kishimoto *J.Appl.Phys* 62, 3751 (1987)

[18] R. V. Ghita, C.Negrila, A.S.Manea, C.Logofatu, M.Cernea, M.F.Lazarescu, *J.Optoelectron.Adv.Mater,* 5, pp.859 (2003)

[19] S. Tanuma, C.J.Powell and D.R.Penn, *Surf.Interface Anal* 21,pp.165 (1994)

[20] S. Tanuma, C.J.Powell and D.R.Penn,*Journal of Electron Spectroscopy and Related Phenomena* 52, pp.285 (1990)

[21] S. Tanuma, C.J.Powell and D.R.Penn, *Surface Science* 192, L 849 (1987)

[22] H. Bethe, *Ann.der Physik*, 5 pp.325 (1930)

[23] http://en.wikipedia.org

[24] C. C. Negrila, C.Cotirlan, F.Ungureanu, C.Logofatu, R.V.Ghita, M.F.Lazarescu, *J.Optoelectron. Adv.Mater*, 10 (6), pp.1379 (2008)

[25] Freiberger General Specifications, issue 200

[26] (www.fem-semcond.com/pdf/gen.spec.pdf)

[27] T. Hou, C.M.Greenlief, S.W.Keller, L.Nelen and J.F.Kauffman, *Chem. Mater.* 9,pp.3181 (1997)

[28] C. C. Negrila, C.Logofatu, R.V.Ghita, C.Cotirlan, F.Ungureanu, A.S.Manea, M.F.Lazarescu, *J.Crystal Growth*, Vol.310, No.7t-9, pp.1576 (2008).

[29] J. L. Sullivan, W.Yu and S.O.Saied, *Surface and Interface Analysis*, Vol.22, pp.515 (1994)

[30] Y. Tu and J. Tersoff, *Thin Solid Films*, Vol.400, No.1-2, pp.95(2001)

[31] Ch. D. Lorenz, M.Tsige, Susan B.Rempe, M.Chandross, M.J.Stevens, G.S.Grest *Journal of Computational and Theoretica* Nanoscience, Vol.7, No.12, pp.2586 (2010)

[32] S. Bergfeld, B.Braunschweig, W.Daum, *Physical Review Letters*, Vol.93, No.9 (2004)
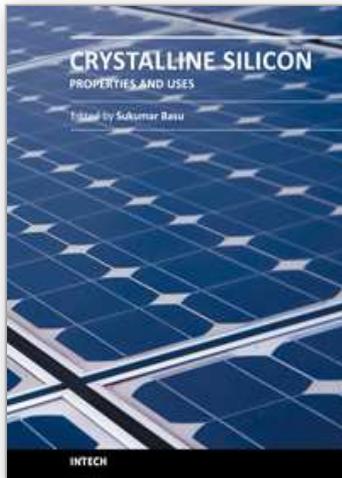
**Crystalline Silicon - Properties and Uses**

Edited by Prof. Sukumar Basu

ISBN 978-953-307-587-7

Hard cover, 344 pages

**Publisher** InTech

**Published online** 27, July, 2011

**Published in print edition** July, 2011

The exciting world of crystalline silicon is the source of the spectacular advancement of discrete electronic devices and solar cells. The exploitation of ever changing properties of crystalline silicon with dimensional transformation may indicate more innovative silicon based technologies in near future. For example, the discovery of nanocrystalline silicon has largely overcome the obstacles of using silicon as optoelectronic material. The further research and development is necessary to find out the treasures hidden within this material. The book presents different forms of silicon material, their preparation and properties. The modern techniques to study the surface and interface defect states, dislocations, and so on, in different crystalline forms have been highlighted in this book. This book presents basic and applied aspects of different crystalline forms of silicon in wide range of information from materials to devices.

**How to reference**

In order to correctly reference this scholarly work, feel free to copy and paste the following:

Rodica Ghita, Constantin Logofatu, Catalin-Constantin Negrila, Florica Ungureanu, Costel Cotirlan, Adrian-Stefan Manea, Mihail-Florin Lazarescu and Corneliu Ghica (2011). Study of SiO2/Si Interface by Surface Techniques, Crystalline Silicon - Properties and Uses, Prof. Sukumar Basu (Ed.), ISBN: 978-953-307-587-7, InTech, Available from: http://www.intechopen.com/books/crystalline-silicon-properties-and-uses/study-of-sio2-si-interface-by-surface-techniques